Bull. Mater. Sci. (2020) 43:41
https://doi.org/10.1007/s12034-019-2019-6

Growth, spectral, mechanical, electrical and optical characterization of guanidinium hydrogen succinate single crystal

K KRISHNARAJ[1], N SIVAKUMAR[2] and P PRAVEEN KUMAR[1,*]
[1]Department of Physics, Presidency College, Chennai 600 005, India
[2]Crystal Growth Centre, Anna University, Chennai 600 025, India
*Author for correspondence (ppkpresidency@gmail.com)

MS received 23 May 2019; accepted 12 September 2019

Abstract. Slow evaporation method was employed to grow an organic crystal: guanidinium hydrogen succinate (GHS). Monoclinic structure of GHS was confirmed by single-crystal X-ray diffraction study and its space group was determined to be $P2_1/c$. Different functional groups present in GHS were estimated qualitatively by Fourier transform infrared analysis. The crystalline quality of the grown GHS was ascertained by high-resolution X-ray diffraction study. The UV–Vis absorption spectrum reveals a lower cut-off wavelength of 235 nm. The minimum absorption shows the wide optical transparency in the entire visible region. Work hardening co-efficient value ($n = 1.7$) shows that the GHS crystal belongs to soft material category. Behaviour of dipoles in the crystal was examined through dielectric study. The third-order nonlinear optical analysis was carried out on GHS crystal through Z-scan technique. The nonlinear refractive index (n_2), nonlinear absorption coefficient (β) and third-order nonlinear optical susceptibility ($\chi^{(3)}$) were estimated to be -5.78×10^{-8} cm^2 W^{-1}, 0.72×10^{-4} cm W^{-1} and 8.09×10^{-6} esu, respectively.

Keywords. Optical material; crystal growth; organic compounds; mechanical properties; optical properties.

1. Introduction

Efficient nonlinear optical (NLO) materials are required for optical devices, particularly in the field of photonic technology and electro-optics. Nowadays, electronic components are replaced by photonic materials in most of the working devices. In the recent past, many of the organic, semi-organic and inorganic materials were discovered for various NLO applications like frequency conversion, optical information processing, optical data storage, optical imaging, etc. [1,2]. Researchers currently focus on the growth of organic NLO materials, because of their quick optical response, structural flexibility and formation of weak van der Waals and extended hydrogen bonds [3]. Organic materials have excellent optical characteristics such as high electronic susceptibility, high molecular polarizability and higher laser damage threshold [4]. Organic materials are more versatile than inorganic materials due to their delocalized π-electron systems, large dipole moment and lack of inverse symmetry [5]. The discovery of dicarboxylic acids is made possible through the development of hydrogen-bonded networks with the other molecules [6]. Succinic acid ($C_4H_6O_4$) is a dicarboxylic acid found in amber, lignite and many plants. It is used as an efficient biodegradable in polymeric compounds and is also involved in the fabrication of high-electron-mobility transistor (HEMT) [7]. The molecular structure and molecular packing of guanidinium hydrogen succinate (GHS) were reported [8]. Guanidine is an excellent material and shows its importance in organic, biological, medicinal chemistry and materials engineering, particularly in NLO optical applications [9–11]. Many of the guanidine complexes were analysed for their NLO behaviour [12,13].

In the present work, attempt has been made to grow GHS crystal by conventional slow evaporation solution growth technique and its crystalline perfection. Optical, mechanical and dielectric studies are analysed and discussed in detail.

2. Experimental

2.1 *Crystal synthesis*

Guanidinium carbonate and succinic acid were taken in 1:2 molar ratio and dissolved completely in deionized water. The mixture was stirred well for 8 h. Successive recrystallization processes were carried out in order to get a homogeneous mixture of impurity-free mother solution for the crystal growth. Well-purified solution was again filtered using a high-quality Whatman filter paper into a beaker and was then kept in a dust-free atmosphere for slow evaporation. Over the period of 30 days, an optically transparent crystal with dimension $19\times16\times3$ mm^3 was harvested. A photograph of the grown GHS crystal is shown in

Published online: 03 January 2020

Figure 1. Photograph of as-grown GHS crystal.

Table 1. Lattice parameter values of GHS single crystal.

Crystal structure data	GHS crystal (present)	Reported [8]
a (Å)	6.564 ± 0.04	6.5710 (10)
b (Å)	18.502 ± 0.11	18.388 (4)
c (Å)	7.250 ± 0.04	7.2300 (10)
Volume (Å^3)	815	799
α	90°	90°
β	112°	112°
γ	90°	90°
Crystal system	monoclinic	monoclinic
Space group	$P2_1/c$	$P2_1/c$

figure 1. GHS was synthesized according to the following reaction:

$$C_3H_{12}N_6O_3 + 2(C_4H_6O_4) \longrightarrow 2(C_5H_{11}N_3O_4) + CO_2 \uparrow + H_2O.$$

3. Results and discussion

3.1 *Single X-ray diffraction and powder X-ray diffraction studies*

GHS crystal of suitable size was selected for single-crystal X-ray diffraction (XRD) analysis to confirm the crystalline nature and unit cell parameters using an ENRAF NONIUS CAD4 X-ray diffractometer instrument. From the XRD data, it is observed that GHS crystallizes in the monoclinic crystal system with the space group of $P2_1/c$. The obtained crystallographic cell parameters are in close relation with the reported value [8] and are given in table 1. The recorded powder X-ray diffraction (PXRD) pattern for GHS crystal along with the simulated pattern is shown in figure 2a and b. The powder pattern was simulated from the CIF (CCDC No 631518–631520) using diamond software. The simulated

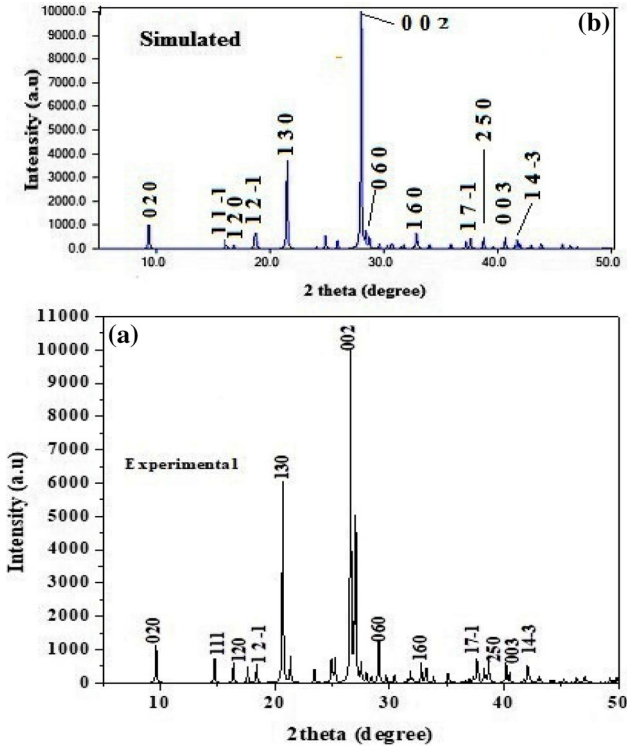

Figure 2. **(a)** Experimental PXRD pattern and **(b)** simulated PXRD pattern of GHS crystal.

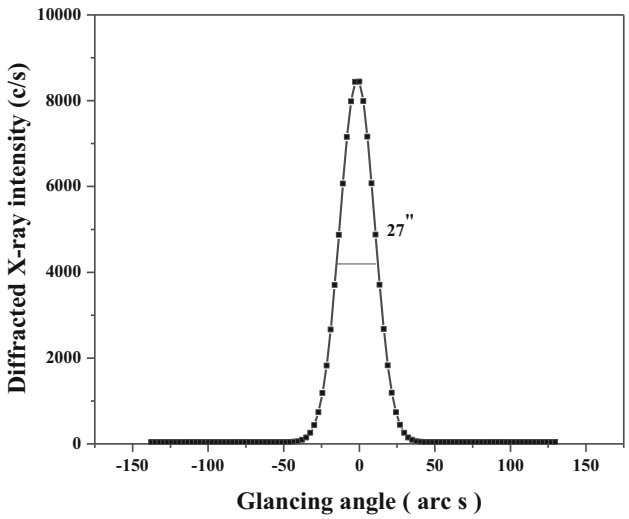

Figure 3. HRXRD curve of GHS crystal.

pattern coincides well with the experimental pattern. The experimental diffraction peaks were indexed using PROZSKI software. The sharp and well-defined peaks indicate the crystalline nature of the GHS compound.

3.2 *High resolution X-ray diffraction*

High-resolution X-ray diffraction (HRXRD) study was employed on the material to understand the crystallinity of

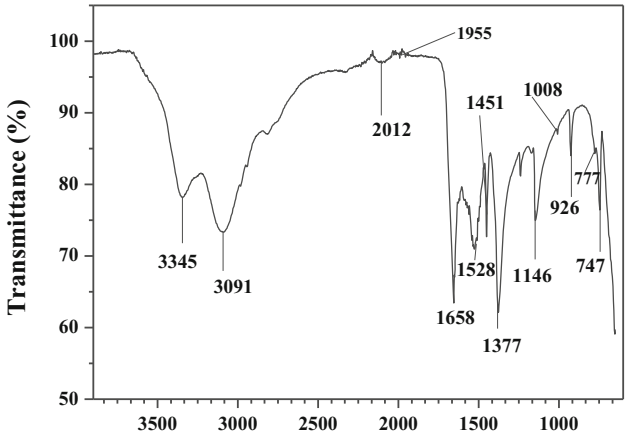

Figure 4. FTIR spectrum of GHS.

GHS. The HRXRD curve is recorded using an Analytical X'Pert PRO MRD XRD system with MoKα_1 radiation and is depicted in figure 3. The diffraction curve contains a single peak without any satellite peaks; this clearly indicates that the grown crystal does not contain any internal structural grain boundaries and the absence of impurities at macroscopic level. The diffraction full-width at half-maximum (FWHM) of the curve is determined to be 27″ and is near the value predicted from the plane wave theory [14].

The single sharp diffraction peak with very low FWHM (27″) reveals that the crystalline quality is fairly good and depicts the low point defect density [15]. Environmental conditions and thermodynamical factors also result in point defects; such things cannot be avoided during growth [16]. The peak broadening of DC curve without much asymmetry about a peak position is attributed to Frankel defects and dislocations in the crystal [17]. However, crystalline materials with low defects cannot disturb the performance of optical devices.

3.3 *Fourier transform infrared spectral studies*

The Fourier transform infrared (FTIR) spectrum of GHS crystal was recorded in the range of 400–4000 cm^{-1} using a Perkin-Elmer Spectrum One FTIR spectrometer. A pellet was prepared from powdered sample with KBr. The observed spectrum is shown in figure 4. The peak at 3345 cm^{-1} indicates the N–H stretching vibration. The O–H stretching mode is observed at 3091 cm^{-1}. The band at 2012 cm^{-1} is attributed to C=N (nitrile) stretching vibration. The peak at 1955 cm^{-1} is attributed to C=O asymmetric stretching vibration of carboxylic group. The intense sharp peak at 1656 cm^{-1} is due to NH_2^+ in-plane bending mode [18]. The peak at 1528 cm^{-1} indicates the N–O stretching vibrations. The peak at 1451 cm^{-1} indicates the C–N stretching vibrations. The band observed at 1377 cm^{-1} is assigned to C–O stretching. The peak at 1148 and 1008 cm^{-1} corresponds to C–O stretching vibration. This confirms the presence of free carboxylate anion, wherein the negative charge is localized on the oxygen atoms in carboxylate anion [13]. The O–H bending mode is observed at 926 cm^{-1}. The sharp peaks at 777 and 747 cm^{-1} are attributed to N–H wagging vibrations. Table 2 shows the spectral and band assignments of GHS crystal.

Table 2. Wave number and their assignments.

Wavenumber (cm^{-1})	Assignment of vibrations
3345	N–H stretching
3091	O–H stretching
2012	C=N (nitrile) stretching vibration
1955	C=O asymmetric stretching
1658	NH_2 in-plane bending mode
1528	N–O stretching
1451	C–H in-plane bending vibration
1377	C–O stretching
1146	C–O stretching
1008	C–O stretching
926	O–H bending mode
777	N–H wagging
747	N–H wagging

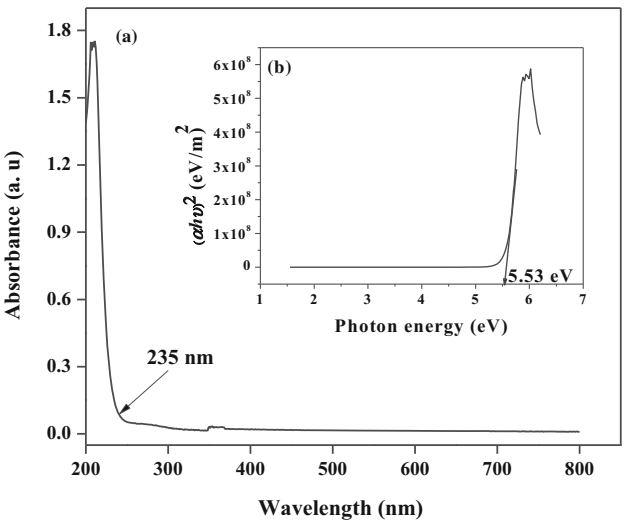

Figure 5. **(a)** UV–Vis absorption spectrum and **(b)** optical band gap energy of GHS crystal.

3.4 *UV–Vis–NIR spectral analysis*

The absorption spectrum of GHS crystal was obtained using a Varian Carry 5E dual-beam spectrophotometer in the range of 200–800 nm. The optical absorbance spectrum is presented in figure 5a. From the spectrum, it is clear that the GHS crystal is highly transparent in the entire visible region (350–750 nm) with the lower cut-off wavelength of 235 nm. Lower absorption of the crystal shows its suitability for NLO applications in the visible region [19].

The optical band gap of the GHS crystal is estimated from the Tauc relation

$$(\alpha h\nu)^2 = A(h\nu - E_g) \quad (1)$$

where α is the absorption coefficient, A is a constant and h is Planck's constant. The plot between $(\alpha h\nu)^2$ and photon energy $(h\nu)$ is shown in figure 5b. Intercept to the x-axis determines the band gap energy (E_g) of the GHS crystal and is estimated to be 5.53 eV. The wide band gap of the grown crystal shows the high transmittance and also ensures that the GHS crystal is suitable for optical harmonic generation and optoelectronic device applications [20].

3.5 *Photoluminescence studies*

Photon emission owing to the excitation of various electronic states by a suitable excitation wavelength reveals the photoluminescence (PL) spectrum [21], which provides information about luminescence property, deeper defects, recombination behaviour and dislocations in the crystal. The excitation wavelength of 235 nm (cut-off measured from UV spectrum) was used to record PL spectrum in the range of 250–500 nm at room temperature using a Jobin Yvon-Spex spectrofluorometer (Fluorolog version-3, Model FL3-11) and is shown in figure 6. A sharp peak at 261 nm observed in the emission spectrum is due to the electron-donating group NH and electron-accepting group COOH. The low value of PL intensity in the longer wavelength region could be due to low barrier of rotation in the carboxylic group around the central C–C bond [22]. The energy of emission peak (4.75 eV) is smaller than the optical band gap energy (5.53 eV) of the material. This suggests that the obtained PL is not involved in the direct electronic transition [23]. Thus, it is clearly noted that the PL emission of the crystal material is associated with trapped electrons and holes present in the localized states between the valence band (VB) and the conduction band (CB). Therefore, the PL spectrum provides information about the band gap energy and the electronic behaviour of the grown crystal.

3.6 *Microhardness analysis*

Microhardness test is a well-known method to find the mechanical property of the crystals and plays a vital role in the optoelectronic device fabrications. The information regarding the deformation characteristics, yield strength, molecular bindings and elastic constant of the materials can be easily studied from the mechanical analysis [24,25]. GHS crystal of suitable size was taken to carry out the hardness study at room temperature using a Leitz Wetzler hardness tester fitted with a Vickers pyramidal indenter.

The Vickers hardness number (H_v) is estimated using the relation

$$H_v = 1.8544(p/d^2)\ \text{kg mm}^{-2} \quad (2)$$

where H_v is the Vickers hardness number in kg mm^{-2}, p is the indentor load in kg and d is the diagonal length of the impression in mm. Figure 7a depicts a plot of H_v number *vs.* load (p) and it is identified that the material exhibits reverse indentation size effect (RISE), i.e., the value of H_v increases with an increase of applied load [26]. The Meyer index number is estimated from Meyer's equation, which relates the load and length of diagonal indentation. According to Meyer's equation

$$p = kd^n \quad (3)$$

where k is material constant and n is Meyer's index number. A plot of log p *vs.* log d shows linear behaviour

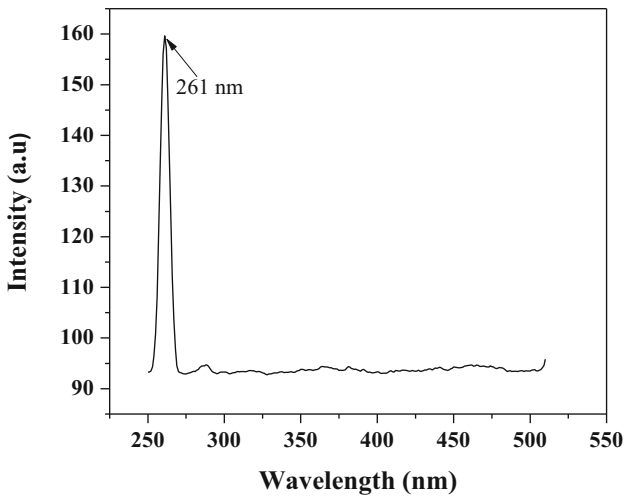

Figure 6. PL emission spectrum of GHS.

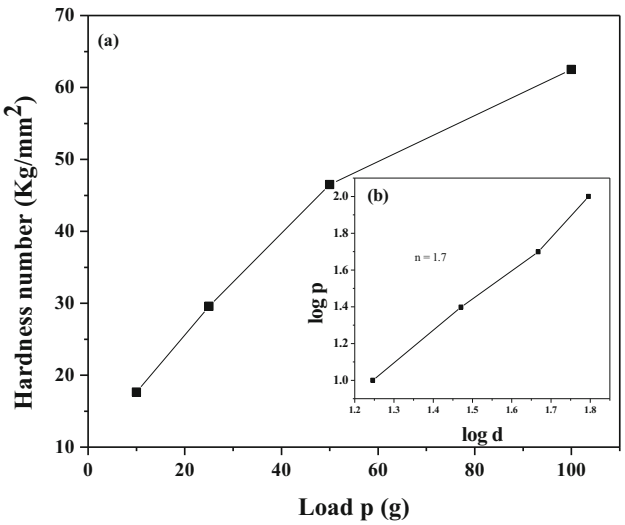

Figure 7. **(a)** Load p *vs.* H_v and **(b)** log d *vs.* log p of GHS.

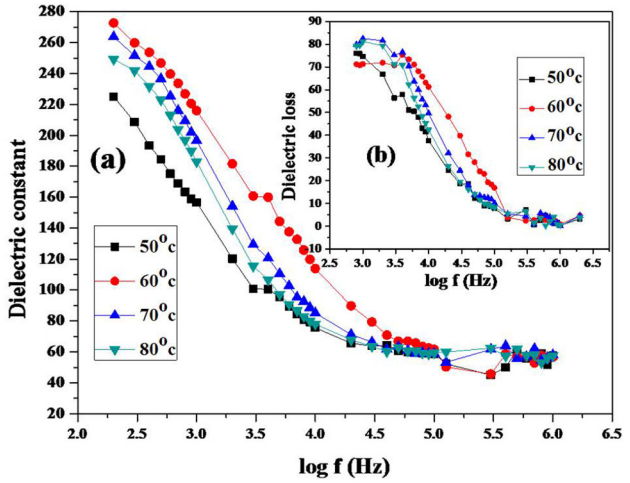

Figure 8. **(a)** Dielectric constant with frequency and **(b)** dielectric loss with frequency of GHS.

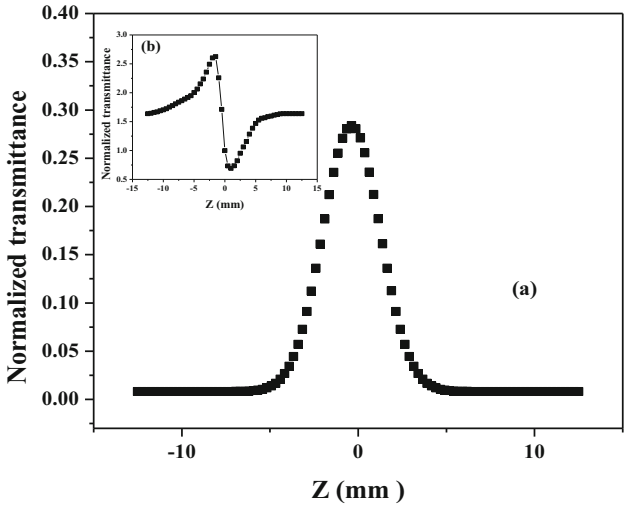

Figure 9. **(a)** Z-scan curve for open aperture and **(b)** Z-scan curve for closed aperture.

and is presented in figure 7b. From the slope, 'n' value is calculated and it is 1.7. According to Onitsch, n should lie between 1 and 1.6 for hard materials and above 1.6 for soft materials [27,28]. Hence, GHS crystal belongs to soft category materials, which can be attributed to high crystal bonding forces of the material. Material hardness also depends on directionality of the bonds, average bond strength and the number of bonds per unit volume [29].

3.7 *Dielectric studies*

The dielectric measurement was taken using a HIOKI 3532-50 LCR HITESTER meter. The dielectric constant and dielectric loss were estimated for varying frequencies at different temperatures, from 50 to 80°C. The dielectric constant is calculated using the equation

$$\varepsilon_r = Ct/(\varepsilon_o A) \tag{4}$$

where t is the thickness of the sample, A is the area of the sample, C is the capacitance of the sample, ε_o is the permittivity of free space and ε_r is the dielectric constant of the sample.

The variation of dielectric constant (ε_r) and dielectric loss as a function of frequency is shown in figure 8a and b. It is observed that the dielectric constant (ε_r) decreases slowly with increasing frequency. The same behaviour is also observed in the case of dielectric loss with frequency. The material exhibits high dielectric constant at low frequencies; it may be due to the space charge, orientation, ionic and electronic polarizations. The low value of dielectric constant at high frequencies can be due to the failure of the afore-mentioned polarizations, i.e., at higher frequencies, the material cannot follow the quick variation of electric field, resulting in cancellation of all types of polarizations [30,31].

The low value of dielectric constant and dielectric loss dictates that the grown crystal has minimum defects with improved optical quality. Thus, the material can be used for wide NLO applications [32,33].

3.8 *Z-scan technique*

Z-scan technique was carried out to study the third-order optical NLO properties of the grown GHS crystal using He–Ne laser of wavelength 632.8 nm as a light source focused by a lens of focal length 22.5 cm. The nonlinear refractive index (n_2), nonlinear absorption coefficient (β) and the third-order nonlinear susceptibility ($\chi^{(3)}$) of the grown crystal were estimated from open and closed aperture Z-scan curve depicted in figure 9a and b.

From the curves, the difference between the normalized peak and valley transmittances is evaluated using the relation

$$\Delta T_{P-V} = 0.406(1-S)^{0.25}|\Delta\Phi_0| \tag{5}$$

where $\Delta\Phi_0$ is the axis phase shift at the focus and S is the linear transmittance of aperture. It can be calculated using the expression

$$S = 1 - \exp\left(\frac{-2r_a^2}{\omega_a^2}\right) \tag{6}$$

where r_a is the radius of aperture and ω_a is the beam radius of the aperture.

The nonlinear refractive index (n_2) is evaluated using the equation [34]

$$n_2 = \frac{\Delta\phi_0}{\kappa L_{eff} I_0} \tag{7}$$

Table 3. Third-order nonlinear optical parameters of GHS single crystal.

Parameters	GHS
Nonlinear refractive index (n_2)	-5.78×10^{-8} (cm^2 W^{-1})
Nonlinear absorption coefficient (β)	0.72×10^{-4} (cm W^{-1})
Real part of the third-order susceptibility (Re $\chi^{(3)}$)	7.40×10^{-6} (esu)
Imaginary part of the third-order susceptibility (Im $\chi^{(3)}$)	3.29×10^{-6} (esu)
Third-order NLO susceptibility ($\chi^{(3)}$)	8.09×10^{-6} (esu)

where κ is the wave number ($\kappa = 2\pi/\lambda$), I_0 is the intensity of the laser beam at the focus ($Z = 0$), $L_{\text{eff}} = [1-\exp(-\alpha L)]/\alpha$ is an effective thickness of the material, α is linear absorption coefficient and L is thickness of the sample. The nonlinear absorption coefficient (β) is calculated from the open aperture Z-scan plot:

$$\beta = \frac{2\sqrt{2}\Delta T}{L_{\text{eff}} I_0}. \tag{8}$$

The real and imaginary parts of the third-order NLO susceptibility ($\chi^{(3)}$) are estimated using the equations [35]

$$\text{Re } \chi^{(3)}(\text{esu}) = \frac{10^{-4}\left(n_2 \varepsilon_0 c^2 n_0^2\right)}{\pi} (\text{cm}^2\ \text{W}^{-1}) \tag{9}$$

and

$$\text{Im } \chi^{(3)}(\text{esu}) = \frac{10^{-2}(\lambda\beta\varepsilon_0 c^2 n_0^2)}{4\pi^2} (\text{cm}^2\ \text{W}^{-1}) \tag{10}$$

where ε_0 is the vacuum permittivity and c is the velocity of light in vacuum. Obtained results from the Z-scan measurement for GHS crystal are presented in table 3.

$$\chi^{(3)} = \sqrt{(\text{Im } \chi^{(3)})^2 + (\text{Re } \chi^{(3)})^2}. \tag{11}$$

Table 3 portrays the results of the Z-scan technique for GHS. This material shows large third-order NLO susceptibility (8.09×10^{-6} esu), which is due to large molecular polarizability of the material. The movement of π-electron cloud present in the crystal is responsible for large molecular polarizability [36,37]. The open aperture curve shows high-intensity transmission and it indicates saturable absorption. The peak followed by the valley of the closed aperture curve indicates the self-defocusing nature of the material. This result is supported well by the negative value of refractive index of the crystal, which is an important property for use in the shielding of optical sensors like night-vision devices [38,39].

4. Conclusion

Single crystal of GHS was grown by slow evaporation method at room temperature. XRD studies reveals that the grown GHS crystal belongs to the monoclinic system with space group of $P2_1/c$. Crystalline perfection was discussed through HRXRD study. The functional groups and chemical bond vibrations were established from FTIR spectral analysis. The lower cut-off wavelength and the optical band gap energy of GHS crystal were determined to be 235 nm and 5.53 eV, respectively. The lower optical absorbance of the crystal confirms its suitability for optical device fabrication. Micro-hardness study depicts that the GHS crystal belongs to soft material category. The enhanced optical quality with low defect density of the materials was identified through dielectric studies. The third-order optical parameters like optical susceptibility, refractive index and absorption coefficient of GHS were estimated by Z-scan technique. All the analyses reveal that the grown material will be a suitable one for the potential optical device processes.

Acknowledgements

The first author, Mr Krishnaraj, acknowledges SAIF, IIT Madras, and VIT University for their facilities provided towards the research work.

References

[1] Zamara A, Rajesh K, Thirugnanam A and Praveen Kumar P 2014 *J. Opt.* **125** 6082
[2] Jagadeesh M R, Suresh Kumar H M and Ananda Kumari R 2015 *J. Opt.* **126** 4014
[3] Kato K 1980 *J. Quantum Electron.* **16** 810
[4] Gayathri K, Krishnan P, Rajkumar P R and Anbalagan G 2014 *Bull. Mater. Sci.* **37** 1589
[5] Chemla D S and Zyss J (eds) 1987 *Nonlinear optical properties of organic molecules and crystals*, vol 1 (New York: Academic) p 23
[6] Jayanalina T, Rajarajan G, Boopathi K and Sreevani K 2015 *J. Cryst. Growth* **426** 9
[7] Zeikus G, Jain M K and Elankovan P 1999 *Appl. Microbiol. Biotechnol.* **51** 545

[8] Videnova-Adrabinska V, Obara E and Lis T 2007 *New. J. Chem.* **31** 287
[9] Ishikawa T and Isobe T 2002 *Chem.: Eur. J.* **8** 552
[10] Fagan P J, Ward M D and Calabrese J C 1989 *J. Am. Chem. Soc.* **111** 1698
[11] Orner B P and Hamilton A D 2001 *J. Incl. Phenom. Macrocycl. Chem.* **41** 141
[12] Arumanayagam T and Murugakoothan P 2013 *J. Cryst. Growth* **362** 304
[13] Sathya D and Sivashankar V 2015 *J. Opt.* **126** 5873
[14] Parthasarathy M and Gopalakrishnan R 2013 *Opt. Mater.* **35** 205
[15] Lal K and Bhagavannarayana G 1989 *J. Appl. Crystallogr.* **22** 209
[16] Bhagavannarayana G, Rajesh P and Ramasamy P 2010 *J. Appl. Crystallogr.* **43** 1372
[17] Senthilkumar K, Moorthy Babu S and Bhagavannarayana G 2011 *J. Appl. Crystallogr.* **44** 313
[18] Sivashankar V, Siddheswaran R and Murugakoothan P 2011 *J. Mater. Chem. Phys.* **130** 323
[19] Revathi V and Rajendran V 2018 *J. Opt.* **154** 234
[20] Amudha M, Madhavan J and Praveen Kumar P 2016 *J. Opt.* https://doi.org/10.1007/s12596-016-0381-y
[21] Dalal J and Kumar B 2016 *Opt. Mater.* **51** 139
[22] Aravindan A, Srinivasan P, Vijayan N, Gopalakrishnan R and Ramasamy P 2007 *J. Cryst. Res. Technol.* **42** 1097
[23] Shanmugam G and Brahadeeswaran S 2012 *Spectrochim. Acta A: Mol. Biomol. Spectrosc.* **95** 177
[24] Mott B W 1956 *Micro-indentation hardness testing* 2nd edn (London: Butterworths)
[25] Westbrook J H 1958 *Flow in rock salt structure* (Report 58-RL 2033, GE Research Laboratory, USA)
[26] Nirosha M, Kalainathan S, Sarveswari S and Vijayakumar V 2014 *Spectrochim. Acta A: Mol. Biomol. Spectrosc.* **123** 78
[27] Sankar D, Praveen Kumar P and Madhavan J 2010 *J. Phys. B* **405** 1233
[28] Onitsch E M 1947 *Mikroscopia* **2** 131
[29] Sivakumar N and Anbalagan G 2016 *Opt. Mater.* **60** 533
[30] Chandran S, Paulraj R and Ramasamy P 2017 *Opt. Mater.* **73** 154
[31] Sivakumar N, Jayavel R, Anbalagan G and Yadav R R 2018 *Opt. Mater.* **80** 177
[32] Praveen Kumar P, Manivannan V, Tamilselvan S, Senthil S, Victor Antony Raj, Sagayaraj P *et al* 2008 *Opt. Commun.* **281** 2989
[33] Sabari Girisun T C and Dhanuskodi S 2009 *J. Cryst. Res. Technol.* **44** 1297
[34] Shanthi A, Krishnan C and Selvarajan P 2014 *Spectrochim. Acta A: Mol. Biomol. Spectrosc.* **122** 521
[35] Bharath D and Kalainathan S 2014 *Spectrochim. Acta A: Mol. Biomol. Spectrosc.* **118** 1098
[36] John Kiran A, Udayakumar D, Chandrasekharan K, Adhikari A V and Shashikala H D 2006 *J. Phys. B: At. Mol. Opt. Phys.* **39** 3747
[37] He C, Yiqun W, Shi G, Duan W, Song W and Song Y 2007 *Org. Electron.* **8** 198
[38] Sudharsana N, Keerthana B, Nagalakshmi R, Krishnakumar V and Guru Prasad L 2012 *J. Mater. Chem. Phys.* **134** 736
[39] Subashini V, Ponnusamy S and Muthamizhchelvan C 2013 *J. Cryst. Growth* **363** 211